


Oocyte orientation selection method based on the minimum strain position in the penetration process

Cite as: J. Appl. Phys. **125**, 154701 (2019); <https://doi.org/10.1063/1.5086320>

Submitted: 19 December 2018 . Accepted: 30 March 2019 . Published Online: 19 April 2019

Yaowei Liu, Maosheng Cui, Yumeng Sun, Zeyang Feng, Yunxiang Bai, Mingzhu Sun, Qili Zhao, and  Xin Zhao



View Online



Export Citation



CrossMark

ARTICLES YOU MAY BE INTERESTED IN

[Quantitative counting of Zn and O atoms by atomic resolution off-axis and in-line electron holography](#)

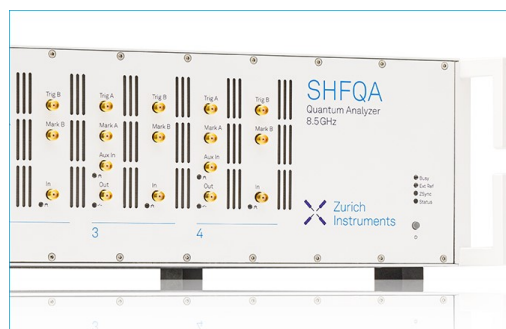
Journal of Applied Physics **125**, 154902 (2019); <https://doi.org/10.1063/1.5075532>

[Theoretical design of coupled high contrast grating \(CHCG\) waveguides to enhance CO₂ light-absorption for gas sensing applications](#)

Journal of Applied Physics **125**, 154502 (2019); <https://doi.org/10.1063/1.5091933>

[Full stress tensor measurement using fluorescence spectroscopy](#)

Journal of Applied Physics **125**, 155105 (2019); <https://doi.org/10.1063/1.5088584>



Learn how to perform the readout of up to 64 qubits in parallel

With the next generation of quantum analyzers on November 17th

Register now

 Zurich Instruments


Oocyte orientation selection method based on the minimum strain position in the penetration process

Cite as: J. Appl. Phys. **125**, 154701 (2019); doi: [10.1063/1.5086320](https://doi.org/10.1063/1.5086320)

Submitted: 19 December 2018 · Accepted: 30 March 2019 ·

Published Online: 19 April 2019



Yaowei Liu,^{1,a)} Maosheng Cui,^{2,a)} Yumeng Sun,¹ Zeyang Feng,¹ Yunxiang Bai,¹ Mingzhu Sun,¹ Qili Zhao,^{1,b)} and Xin Zhao^{1,b)} 

AFFILIATIONS

¹Institute of Robotics and Automatic Information System and the Tianjin Key Laboratory of Intelligent Robotics, Nankai University, Tianjin 300071, China

²Institute of Animal Sciences, Tianjin 300112, China

^{a)}**Contributions:** Y. Liu and M. Cui contributed equally to this work.

^{b)}**Authors to whom correspondence should be addressed:** zhaoqili@nankai.edu.cn and zhaoxin@nankai.edu.cn

ABSTRACT

In this paper, we proposed an oocyte orientation selection method based on the minimum strain position in the penetration process in order to maximize the developmental potential of the operated oocytes. Considering the symmetry of an oocyte during the penetration process, we analyzed only the intracellular strain of the lower half of the oocyte (from 3 o'clock to 9 o'clock). Firstly, the strain distribution in the penetration process was calculated using the finite element analysis method. The influences of penetration force, zona pellucida thickness, oocyte radius, Young's modulus of the cytoplasm, and zona pellucida on the strain distribution were studied. The simulation results showed that the strain values at the 4 o'clock and 9 o'clock areas were significantly smaller than those at the 5 o'clock, 6 o'clock, 7 o'clock, and 8 o'clock areas. Secondly, the experimental strain distribution during penetration was evaluated for the first time using an optical flow method. The experimental strain distribution was strongly positively correlated to the aforementioned simulated results. Finally, the developmental potential of the penetrated porcine oocyte with different orientations was evaluated using the cleavage rate (48 h after penetration and parthenogenetic activation). The cleavage rate was strongly negatively correlated to the intracellular strain. We inferred that a smaller strain on the polar body areas in the penetration process caused less potential damage, which leads to a higher developmental potential of the penetrated oocyte. The optimized oocyte orientations, with the polar body at the 4 o'clock and 9 o'clock areas, are determined based on the minimum strain position in the penetration process.

Published under license by AIP Publishing. <https://doi.org/10.1063/1.5086320>

I. INTRODUCTION

Oocyte penetration has been playing important roles in many cell manipulations, such as nuclear transfer (NT),^{1–4} embryo microinjection,^{5–7} and intracytoplasmic sperm injection (ICSI).^{8–10} Although the success rate of oocyte penetration is very high now (e.g., success rate: 90% in Ref. 11), the developmental potential of the operated cells/embryos has not been significantly improved. For example, Mattos automatically injected the blastocyst, which resulted in a 20% yield of chimeras that was slightly lower than the manual blastocyst microinjections (22.2%).¹² During the penetration process, the oocyte suffers tremendous deformation leading to

huge intracellular strain. Some literature studies have reported that strain could reduce the cell's developmental potential. For example, Scott *et al.* reported that apoptosis may occur in response to short-term, high strain mechanical loading.¹³ Gladman *et al.* have proved that the mechanical deformation could affect the spinal nerves and their associated dorsal root ganglion cells.¹⁴

Oocyte orientations in the penetration process, which are usually denoted by the polar body positions, have also been found to affect the developmental potential. For example, some researchers found that different polar body positions in the penetration process resulted in different developmental potentials of the

oocytes in ICSI.^{15,16} Van der Westerlaken *et al.* found that the oocytes injected with the polar body at 6 o'clock (36%) in ICSI had a higher pregnancy rate than those with other directions.¹⁵ Rienzi *et al.* found that the misalignment between the meiotic spindle and the first polar body predicted an increased risk of fertilization abnormalities.¹⁶ Thus, we hypothesized that reducing the strain at the polar body position during penetration may result in a higher developmental potential of the oocytes.

In this paper, we simulated the penetration process by the finite element analysis method. For the first time, the influences of penetration force, thickness of zona pellucida, radius of the oocyte, Young's modulus of the cytoplasm, and zona pellucida on the strain distribution were studied. The simulation results showed that the strain values at the 4 o'clock and 9 o'clock areas were significantly smaller than those at the 5 o'clock, 6 o'clock, 7 o'clock, and 8 o'clock areas. Secondly, using the optical flow method, we calculated the experimental intracellular strain for the first time. The obtained results showed that the strain values at the 4 o'clock and 9 o'clock areas were also significantly smaller compared with those at the 5 o'clock, 6 o'clock, 7 o'clock, and 8 o'clock areas. The measured strain distribution was strongly positively correlated to the aforementioned simulated strain distribution. Furthermore, we cultured the penetrated porcine oocytes with different orientations. The orientation of the penetrated oocyte was defined as the clock position of the polar body in the focal plane. The developmental potential of the porcine oocytes was evaluated using the cleavage rate of the oocyte at 48 h after parthenogenetic activation.^{17,18} The results showed that the cleavage rate of the penetrated oocyte with the polar body at the 4 o'clock and 9 o'clock positions was significantly higher than that with the polar body at other positions. We concluded that the developmental potential of the porcine oocytes increased as the intracellular strain decreased. We inferred that a smaller strain on the polar body around 4 o'clock and 9 o'clock in the penetration process caused less potential damage on the oocyte, finally leading to a higher developmental potential. The optimized oocyte orientations are determined based on the minimum strain position in the penetration process.

II. METHODS AND MATERIALS

A. Finite element analysis simulation method

To simulate the penetration process by the finite element analysis method, we first measured Young's modulus of zona pellucida (ZP) and the cytoplasm of the porcine oocytes (Fig. 1).

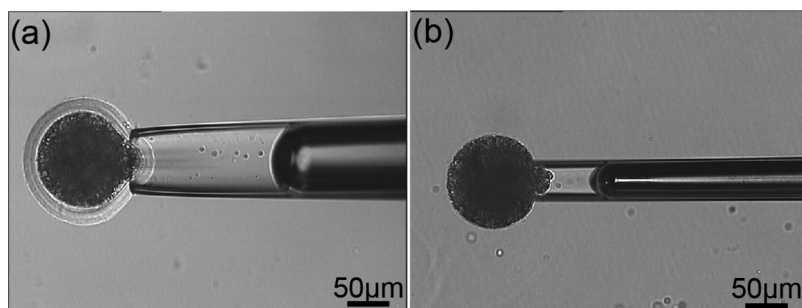


FIG. 1. (a) Measuring Young's modulus of the zona pellucida (ZP). (b) Measuring Young's modulus of the cytoplasm.

The Shell model, which models the oocyte as a compressible, homogeneous, elastic layer with a finite thickness overlaying an isotropic homogeneous elastic cytoplasm, was used to measure Young's modulus of ZP (see Appendix A for more details).^{19–21} Young's modulus of ZP can be estimated as

$$E = 2C(h^*)(1 - \nu^2) \left(\frac{\Delta P}{\Delta L/R_p} \right), \quad (1)$$

where ν is the Poisson ratio, h^* represents oocyte's dimensionless thickness, which is defined as the ratio of the ZP's thickness (h) to the micropipette's radius (R_p), and $C(h^*)$ is a function of h^* . We assumed the ZP and the cytoplasm to be incompressible and the volume remained unchanged when deformed, so ν is set as 0.5.

The half-space model, assuming the cytoplasm as an isotropic, incompressible, elastic half-space medium, was used to measure Young's modulus of the cytoplasm (see Appendix A for more details).^{21,22} To get the cytoplasm out from the surrounded ZP, oocytes were immersed in "proteinase K" for 1 min. During this period, the ZP was dissolved and the cytoplasm without ZP was obtained. Young's modulus of the cytoplasm can be estimated according to

$$E = \Phi \frac{3}{2\pi} \left(\frac{\Delta P}{\Delta L/R_p} \right), \quad (2)$$

where ΔP is the suction pressure, ΔL is the increment with the changing of the aspiration pressure, R_p is the micropipette's radius, Φ is a term that weakly depends on the ratio of the thickness of the micropipette-wall to the radius of the micropipette, and Φ is set as 2.1 in our experiment.

Young's modulus of ZP was measured as 20 ± 4.6 kPa ($n = 15$), Young's modulus of the cytoplasm was measured as 784 ± 50.3 Pa ($n = 15$), the radius of the oocyte was measured as 80 ± 5 μm ($n = 100$), and the thickness of ZP was measured as 20 ± 5 μm ($n = 100$) (see Appendix B for more details about the measuring results). Then, the cell deformation during penetration was simulated by ANSYS Student (Fig. 2):

Step 1: Materials setting: We defined ZP and cytoplasm as structural, linear, elastic, and isotropic materials based on the Shell model and the half-Space model. We set Young's modulus of ZP as 15 kPa, 20 kPa, and 25 kPa, respectively, based on the measured results. We set Young's modulus of the cytoplasm as 730 Pa, 784 Pa, and 830 Pa, respectively. To judge the effect of Young's

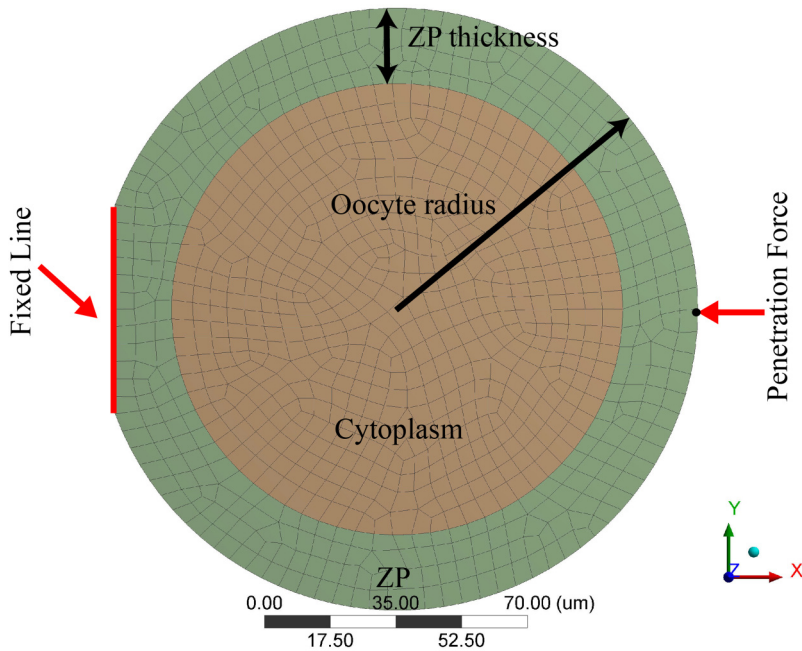


FIG. 2. The structure model used in the finite element analysis. ZP, zona pellucida.

modulus on the intracellular strain, different values of Young’s modulus of ZP and cytoplasm were tried.

Step 2: Geometry construction: We set the radius of the oocyte as 75 μm, 80 μm, and 85 μm, respectively, based on the measured results. We set the thickness of the zona pellucida as 15 μm, 20 μm, and 25 μm, respectively. Set the holding part fixed, and the value was 55.6 μm. To judge the effect of the oocyte radius and ZP thickness on intracellular strain, different values of oocyte radius and ZP thickness were tried.

Step 3: Constraint condition: We assumed that the cytoplasm and the zona pellucida were bonded to each other. Different values of penetration force, 0.5×10^{-5} N, 1×10^{-5} N, 1.5×10^{-5} N, 2×10^{-5} N, 2.5×10^{-5} N, and 3×10^{-5} N, were exerted along the $-X$ direction according to the point-load model (see Appendix C for more details about the point-load model).²³ We set the penetration force to be exerted at the central point on the ZP surface of oocytes.

B. Porcine oocyte penetration experimental method

We rotated the oocyte to move the polar body to the desired clock position using the previous developed cell rotation

method²⁴ and penetrated the oocyte through visual detection and motion control.

The Hough transform algorithm²⁵ was used to locate the oocyte [Fig. 3(a)]. As the porcine oocytes usually have spherical shapes, the Hough transform is utilized to detect cell contour cycle. Using detected cycle, the cell center coordinate (X_O , Y_O) and the oocyte radius R were determined. The injection micropipette (IM) tip position (X_I , Y_I) is located using the template matching method.^{26,27} The poking depth is set as three quarters of the diameter to ensure that the oocytes could be penetrated [Fig. 3(b)]. The coordinate of the starting point and the ending point of micropipette during the penetration process were calculated by

$$\begin{cases} X_{start} = X_O + \frac{5}{4}R, Y_{start} = Y_O, \\ X_{end} = X_O - \frac{1}{4}R, Y_{end} = Y_O. \end{cases} \quad (3)$$

C. Intracellular strain calculation method

The edge detection^{28,29} was utilized to obtain the cell area. The intracellular points were evenly selected in the cell area for intracellular strain calculation (see Fig. 4). Optical flow approach

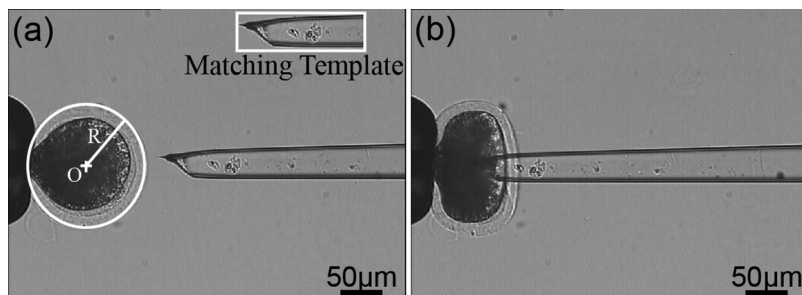


FIG. 3. (a) Determination of the penetration point through visual detection. (b) Penetrating to the center of the oocyte.

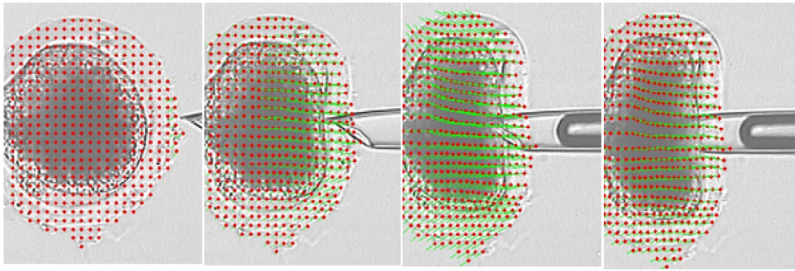


FIG. 4. Positioning the tracking points at different penetration stages.

was used to detect the positions of the intracellular points.³⁰ Then, the velocities of all the points were calculated by the positions of the intracellular points in the adjacent two frames. Figure 4 shows the positions of the intracellular points at different penetration stages. The red points stand intracellular points, while the green lines show the velocities of the points.

Finally, the strain distribution of the oocyte was obtained by calculating the ratio of the variation of the distance between two adjacent points to their initial distance. The strain between two adjacent points was obtained by

$$\varepsilon = \lim_{L \rightarrow 0} \frac{\Delta L}{L}, \quad (4)$$

where L is the initial distance between the two adjacent points and ΔL is the distance variation after the deformation. Since the deformation and strain of the oocytes occurred mainly in the horizontal direction, we only calculated the horizontal component of the strain given in Eq. (4).

D. Parthenogenetic activation

The oocytes were washed three times in phosphate buffer saline (PBS) solution, then gradually equilibrated in activation medium after being penetrated. For activation, the oocytes were placed between electrodes covered with activation medium in a chamber connected to a BTX (CF-150B, Biological Laboratory Equipment, Maintenance and Service Ltd). Oocytes were activated with a single direct current pulse with an electrical intensity of 120 V/cm for 100 μ s. Then, the oocytes were washed three times in porcine zygote medium-3 (PZM-3), placed into 50 μ l PZM-3 droplets covered with mineral oil, and then cultured at 39 °C.

III. STATISTICAL ANALYSIS

Data were evaluated by one-way analysis of variance (ANOVA) with Tukey's test for comparisons between groups using IBM SPSS Statistics 20 and were expressed as mean \pm SEM. A P value less than 0.05 was considered as a significant difference.

IV. ETHICAL STATEMENT

All the procedures were approved by the Animal Care and Use Committee of Tianjin Animal Science and Veterinary Research Institute and were performed in accordance with the NIH Guide for the Care and Use of Laboratory Animals (No. 8023, revised in 1996).

V. SYSTEM OVERVIEW

The experiment in this paper was performed on the self-developed NK-MR601 micro-operation system (Fig. 5).^{31–35} The system consists of an optical microscope (CK-40, Olympus); a CCD camera (W-V-460, Panasonic) for the acquisition of the real-time image at 30 frame/s; a motorized X-Y stage (with a travel range of 100 mm with a repeatability of $\pm 1 \mu$ m/s and a maximum speed of 2 mm/s); a pair of XYZ manipulators (travel range of 50 mm with a repeatability of $\pm 1 \mu$ m/s and a maximum speed of 1 mm/s); an in-house developed micro-injector provides the negative and positive pressure; an in-house developed motion control box controls the microplatform, micromanipulators, and micro-injector through the host computer.

The holding micropipette (HM) was made from borosilicate glass tubes with an outer diameter of 1 mm and an inner diameter of 0.6 mm. The holding micropipettes were pulled by the puller (MODEL P-97, Sutter Instrument) and fractured by the microforge

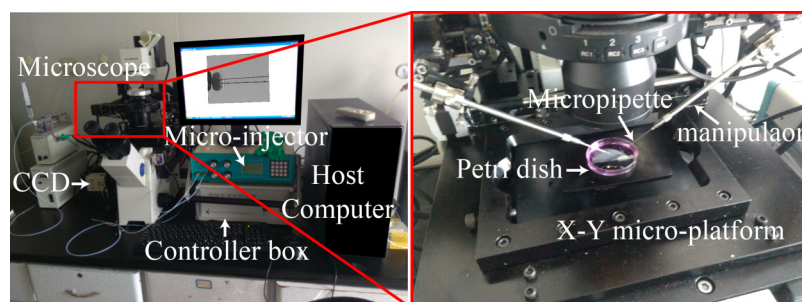


FIG. 5. NK-MR601 micro-operation system.

(MF-900, NARISHIGE) to generate a micropipette with a diameter of 50–80 μm . Then, the HM was melt by alcohol lamp through the professional operator to smooth the tip opening. The injection micropipette (IM) was bought from CooperSurgical (TPC, LBC-OD20BA90) with the diameter of 20 μm and a slope angle of 45°.

VI. EXPERIMENTS AND RESULTS

A. Simulated intracellular strain distribution

As the injection micropipette penetrated the oocyte along the $-X$ direction, the oocyte deformation mainly occurred in the horizontal direction. Thus, we ignored the vertical cell deformation and only considered the strain in the horizontal direction. Figure S1 in the [supplementary material](#) showed the simulated strain distribution in the oocytes with different penetration forces. In the simulation, the oocyte radius, ZP thickness, Young's modulus of ZP, and the cytoplasm were set as 80 μm , 20 μm and 20 kPa and 784 Pa, respectively (see the [supplementary material](#)). The simulated results showed that the strain distribution under different forces was completely consistent. Thus, we only analyzed the strain distribution when the penetration force was set as 2×10^{-5} N.

Considering the symmetry, we only analyzed the intracellular strain of the lower half of the cell [Fig. 6(a)]. The statistical results were shown in Fig. 6(b) (see Fig. S2 in the [supplementary material](#)

for more details). The simulated intracellular strain values at the 4 o'clock and 9 o'clock areas were significantly smaller than those at other areas ($P < 0.05$). The simulated intracellular strain increased from the 4 o'clock area to the 6 o'clock area and decreased from the 7 o'clock area to the 9 o'clock area.

We varied Young's modulus of ZP and cytoplasm and retained the oocyte radius and ZP thickness unchanged (oocyte radius: 80 μm ; ZP thickness: 20 μm). Figures 6(c) and 6(d) showed two representative results with different Young's modulus of ZP and cytoplasm (see Figs. S3 and S4 in the [supplementary material](#) for more details). Then, we varied the radius of oocytes and the thickness of ZP and retained Young's modulus of ZP and cytoplasm unchanged (Zp: 20 kPa; cytoplasm: 784 Pa). Figures 6(e) and 6(f) showed two representative results with different oocyte radius and ZP thickness (see Figs. S5 and S6 in the [supplementary material](#) for more details). The simulated results all showed that the strain values at the 4 o'clock and 9 o'clock areas were also significantly smaller than those at other areas ($P < 0.05$). The intracellular strain increased from 4 o'clock to 6 o'clock and decreased from 7 o'clock to 9 o'clock.

Above all, we could conclude that the simulated strain values at the 4 o'clock and 9 o'clock areas were significantly smaller than those at the 5 o'clock, 6 o'clock, 7 o'clock, and 8 o'clock areas ($P < 0.05$). The intracellular strain increased from 4 o'clock to 6 o'clock and decreased from 7 o'clock to 9 o'clock.

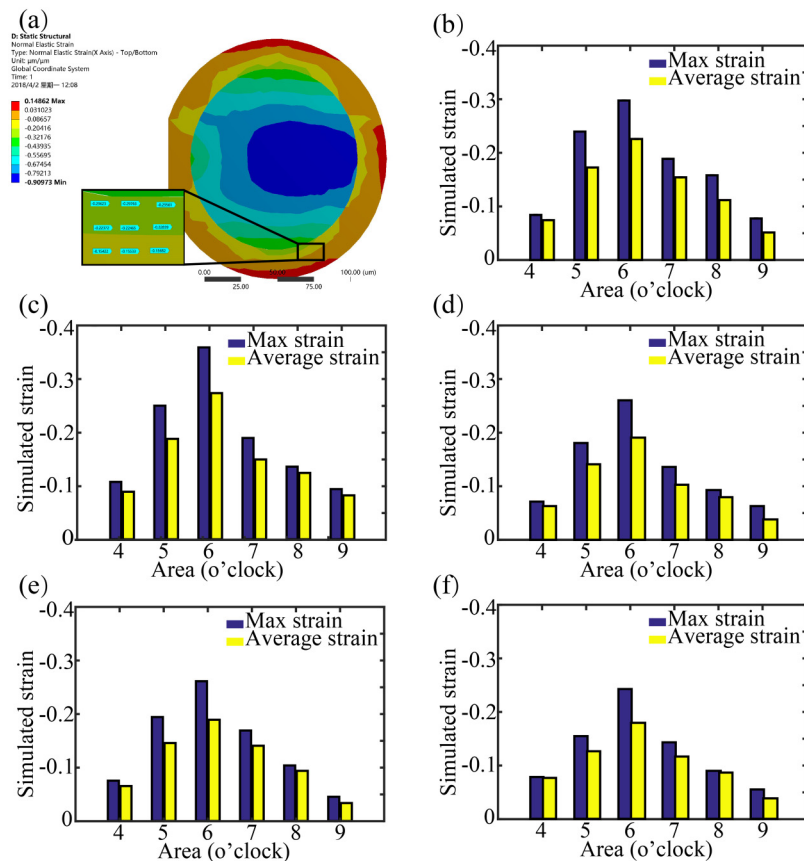


FIG. 6. (a) The simulated strain distribution. (b) The statistical results with Young's modulus of ZP: 20 kPa, cytoplasm: 784 Pa, oocyte radius: 80 μm , ZP thickness: 20 μm . (c) The statistical results with Young's modulus of ZP: 15 kPa, cytoplasm: 730 Pa. (d) The statistical results with Young's modulus of ZP: 25 kPa, cytoplasm: 830 Pa. (e) The statistical results with oocyte radius: 75 μm , ZP thickness: 15 μm . (f) The statistical results with oocyte radius: 85 μm , ZP thickness: 25 μm .

B. Experimental intracellular strain distribution

Six groups of porcine oocytes (10 oocytes in each group) were penetrated. The porcine oocytes in different groups were penetrated with the polar body at the 4 o'clock, 5 o'clock, 6 o'clock, 7 o'clock, 8 o'clock, and 9 o'clock positions, respectively.

The oocytes were penetrated at a speed of $50\ \mu\text{m/s}$, and the strain distribution was calculated using the aforementioned optical flow method [Fig. 7(a)]. Six 3×3 areas at the 4 o'clock, 5 o'clock, 6 o'clock, 7 o'clock, 8 o'clock, and 9 o'clock positions were selected to study the strain in each clock position [Fig. 7(b)]. The maximum and average strain values in each area were calculated (see Fig. S7 in the supplementary material for the normalized histograms) as shown in Fig. 8. The statistical results revealed that the experimental intracellular strain values at the 4 o'clock and 9 o'clock areas were significantly smaller than those at other areas ($P < 0.05$). The experimental intracellular strain values also increased from 4 o'clock to 6 o'clock and decreased from 7 o'clock to 9 o'clock.

We calculated the correlation coefficient between the maximum and average experimental strain and the maximum and average simulated strain: 0.9178 and 0.9303, which demonstrated that the experimental and simulated strain was strongly correlated.

C. Cleavage rate with the different orientations

A total number of 1800 porcine oocytes were selected to perform penetration experiments. These cells were divided into six groups (300 cells/group) according to the polar body position in penetration (4–9 o'clock positions). Each group is named according to the polar body clock position of cells (Groups 4–9). In each group, the cells are further divided into three subgroups (100 cells/subgroup) according to the penetration speed ($10\ \mu\text{m/s}$, $20\ \mu\text{m/s}$, and $50\ \mu\text{m/s}$).

The oocyte was first rotated to move the polar body to the desired clock position, and then penetrated according to the process introduced in II(B); see Fig. 9 (Multimedia view). The penetrated cells were activated and cultured for 48 h. The cleavage rates of the

embryos were shown in Fig. 10 (see Tables I–III in Appendix D for the detailed data).

Experiment results showed that the cleavage rate decreased from Group 4 to Group 6 and increased from Group 7 to Group 9 under different penetration speed, and the cleavage rate increased as the penetration speeds increased. When the penetration speed was $50\ \mu\text{m/s}$, the cleavage rate of Group 4^(a) and Group 9^(a) was significantly higher than that of Group 5^(ab), Group 6^(bc), Group 7^(c), and Group 8^(ab). When the penetration speed was $20\ \mu\text{m/s}$, the cleavage rate of Group 4^(a) and Group 9^(a) was significantly higher than that of Group 5^(ab), Group 6^(ab), Group 7^(b), and Group 8^(ab). When the penetration speed was $10\ \mu\text{m/s}$, the cleavage rate showed no significant difference among groups. However, the cleavage rate of Group 4 and Group 9 was still slightly higher than the other groups.

The correlation coefficient between the cleavage rate and experimental maximum strain, experimental average strain, simulated maximum strain, simulated average strain are -0.8376 , -0.8499 , -0.5605 , and -0.6271 , respectively ($50\ \mu\text{m/s}$ group). The results showed that both the simulated and the experimental strain were strongly negatively correlated to the cleavage rate. We inferred that the developmental potential increased as the intracellular strain decreased.

D. Discussion

In the finite element analysis simulation, we crudely defined the materials as linear, elastic, and isotropic material materials. The motive of using this simple assumption is expending the applicability of our method and results. If the simulated results in these conditions were still similar with the experimental results, our method will be of more universal significance. Fortunately, both the simulated and the experimental intracellular strain increased from the 4 o'clock area to the 6 o'clock area and decreased from the 7 o'clock area to the 9 o'clock area. The intracellular strain was strongly negatively correlated with the cleavage rate. The results showed that these assumptions are suitable.

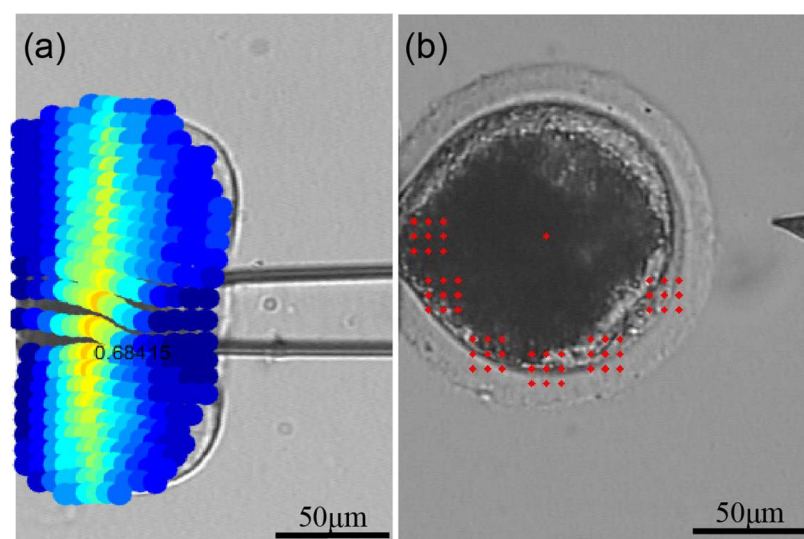


FIG. 7. (a) Experimental intracellular strain distribution with the largest deformation in the penetration process. (b) Six 3×3 areas at 4 o'clock, 5 o'clock, 6 o'clock, 7 o'clock, 8 o'clock, and 9 o'clock to analyze the intracellular strain at each areas.

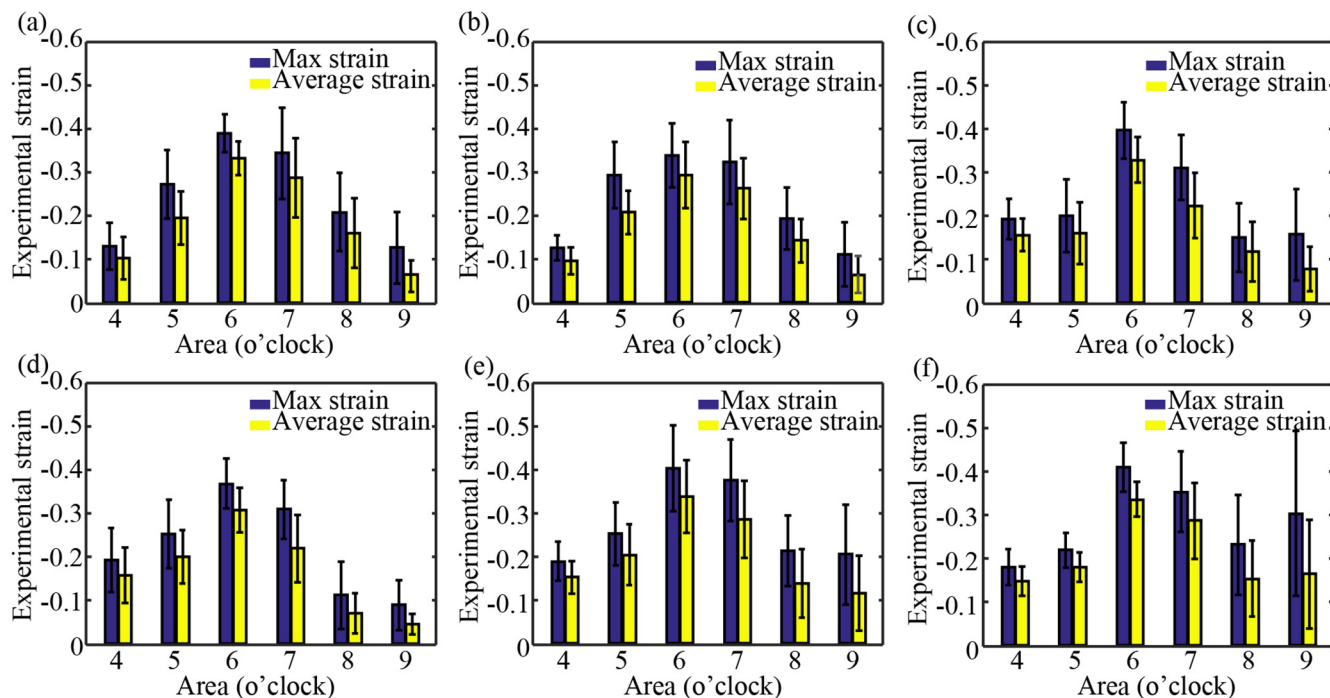


FIG. 8. The statistical results of the experimental strain in each area when penetrated the oocytes with different orientations (penetrate the oocytes with the polar body at the 4 o'clock, 5 o'clock, 6 o'clock, 7 o'clock, 8 o'clock, and 9 o'clock areas).

We compared our results with the previous theoretical predictions. A. A. Boulbitch deduced the expression of the free energy describing small local deflections of a cell membrane and simplified the expression assuming the membrane as quasiflat.³⁶ They found

that under the applied localized force, the local bending of a curved membrane was always followed by its local stretching. In our study, the strain on the zona pelludica (ZP) indicated that there was also bending and stretching at the same time. Considering the ZP in

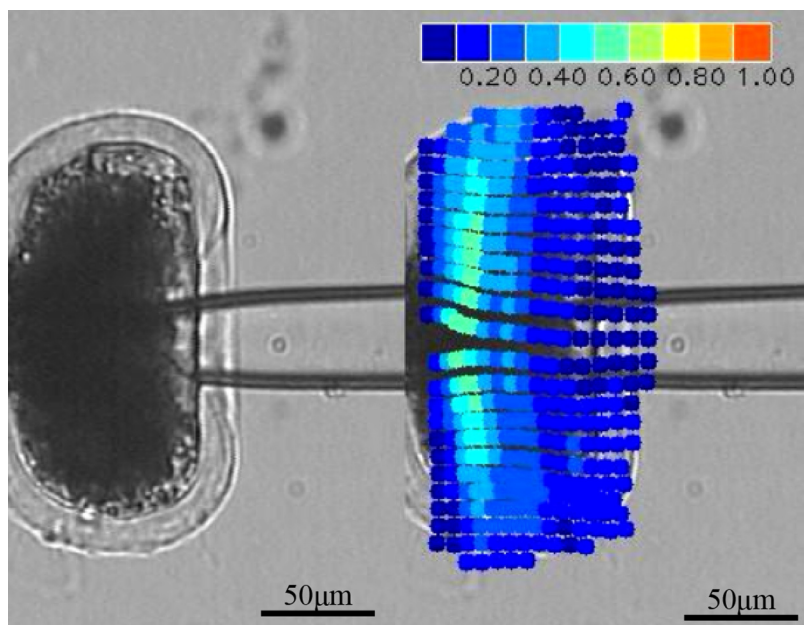


FIG. 9. The strain distribution with the penetration speed of 20 μm/s. Multimedia view: <https://doi.org/10.1063/1.5086320>

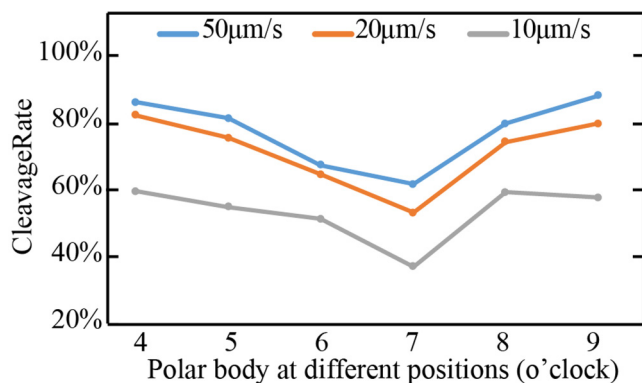


FIG. 10. Average cleavage rate at the penetration speed of $10\ \mu\text{m/s}$, $20\ \mu\text{m/s}$, and $50\ \mu\text{m/s}$ with different oocyte orientations.

our work was much thicker than the membrane in Boulbitch's study, the results of the two methods are considered as consistent with each other.

From Evans, we have learned that the deformation of the biological membrane was nonuniform over the membrane, and the internal dissipation of mechanical energy as heat would limit the rate at which the membrane material deformed as a solid structure.³⁷ We found that the simulated strain and the experimental strain was not identical in this paper. The reason might be that the material assumptions were set crudely. Some researchers defined ZP as more complex material to describe the character of ZP more accurately. For example, Tan *et al.* treated ZP as nonlinear Mooney-Rivlin material.³⁸ Ladjal *et al.* assumed the overall cell as a homogeneous hyperelastic model.³⁹ Our future work will improve the simulation accuracy by adjusting the materials.

There were some interesting findings in the experiments. We found that the simulated strain was significantly smaller when Young's modulus of ZP was bigger; however, the simulated strain showed no significant difference when we changed Young's modulus of the cytoplasm. Meanwhile, the simulated strain was significantly smaller when the thickness of ZP was smaller; however, the simulated strain showed no significant difference when we changed the radius of the oocytes. We inferred that the thickness of ZP and Young's modulus of ZP could affect intracellular strain in the oocyte and further have influence on the developmental potential of the oocytes. Our results were consistent with the findings that the zona pellucida thickness and elasticity could affect the embryos developments.^{40,41}

We compared our results with a previous study. Liu *et al.* investigated the mechanical damage of the cell by counting the number of ruptured bonds.⁴² They found that although the larger velocity caused the larger injection force, the smaller velocity generates more number of ruptured bonds.^{43,44} So, the larger velocity caused less damage, and the cells had better developmental potential. Meanwhile, we found that the cleavage rate of the porcine oocyte increased as the penetration speed increased, which was consistent with their findings.

VII. CONCLUSION

This paper proposed an oocyte orientation selection method based on the minimum strain position in the penetration process. In this study, the penetration process with different parameters was simulated by the finite element analysis method. The experimental intracellular strain in the penetration process was calculated using the optical flow method. Both the simulated strain and the experimental strain were significantly smaller at the 4 o'clock and 9 o'clock areas than those at other areas. The developmental potential of the porcine oocyte was evaluated using the cleavage rate (48 h after penetration and parthenogenetic activation). The experimental results showed that the cleavage rate was significantly higher when we penetrated the oocyte with the polar body at the 4 o'clock and 9 o'clock areas than the 5 o'clock, 6 o'clock, 7 o'clock, and 8 o'clock areas, and the cleavage rate was strongly negatively correlated to the intracellular strain. The developmental potential increased by 61.51% ($10\ \mu\text{m/s}$ group), 54.09% ($20\ \mu\text{m/s}$ group), and 40.13% ($50\ \mu\text{m/s}$) after the oocyte orientation selection. The method could increase the efficiency of oocyte penetration and reduce the dead oocytes in animal clone, ICSI, genetic microinjection, and so on. Meanwhile, this paper opened a door to explore the relationship between a cell's developmental potential and cell orientation in manipulation.

SUPPLEMENTARY MATERIAL

See the [supplementary material](#) for the complete simulated strain distribution with different penetration forces, different Young's modulus of ZP and cytoplasm, different oocyte radius, and ZP thickness.

ACKNOWLEDGMENTS

This research was jointly supported by the National Key R&D Program of China (No. 2018YFB1304900), the National Natural Science Foundation of China (NNSFC, Nos. U1813210 and U1613220), and the Natural Science Foundation of Tianjin (Nos. 14JCZDJC31800 and 14ZCDZGX00801). We declare no competing interests.

APPENDIX A: YOUNG'S MODULUS MEASUREMENT

We used the widely used Shell model (Fig. 11) to estimate Young's modulus of zona pellucida (ZP).^{19–21} In this model, the ZP of the oocyte was assumed as a homogeneous, elastic layer and the stiffness of the cytoplasm was assumed as zero.

Young's modulus of ZP was quantified through the fitted slope of the aspiration pressure vs the normalized aspiration length L_p/R_p . Figure 12 shows the fitted slope when Young's modulus of ZP is 15.6 kPa.

We used the half space model (Fig. 13) to estimate Young's modulus of the cytoplasm.^{21,22} In this model, the cytoplasm was assumed as an isotropic, incompressible, elastic half-space medium.

Young's modulus of the cytoplasm was also quantified through the fitted slope of the aspiration pressure vs the normalized aspiration length L_p/R_p . Figure 14 shows the fitted slope when Young's modulus of the cytoplasm is 762 Pa.

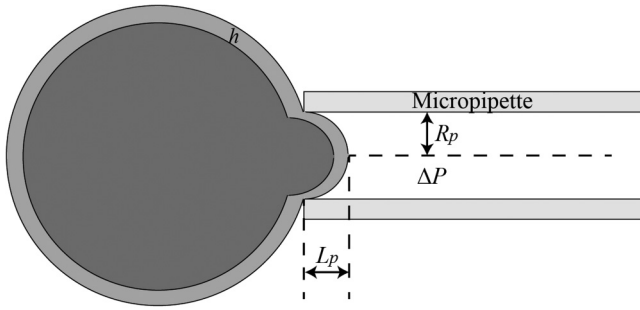


FIG. 11. The Shell model used to estimate Young's modulus of ZP.

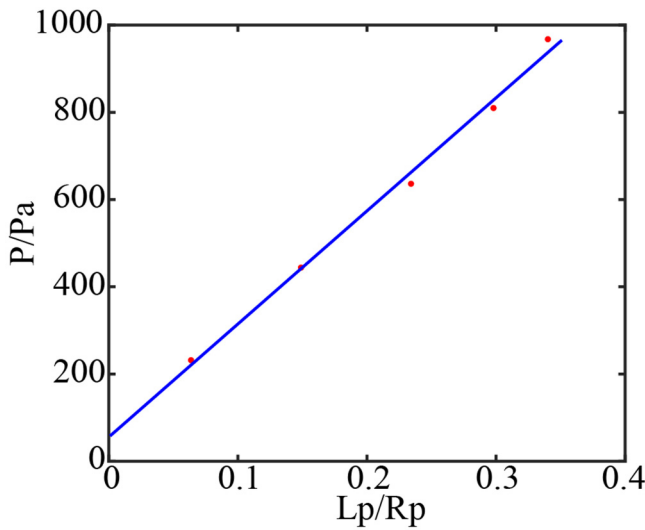


FIG. 12. The relationship between the holding pressure and the elongation of the ZP when its Young's modulus is detected as 15.6 kPa.

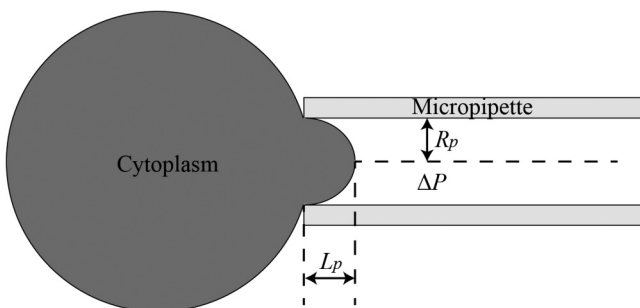


FIG. 13. The half space model used to estimate Young's modulus of the cytoplasm.

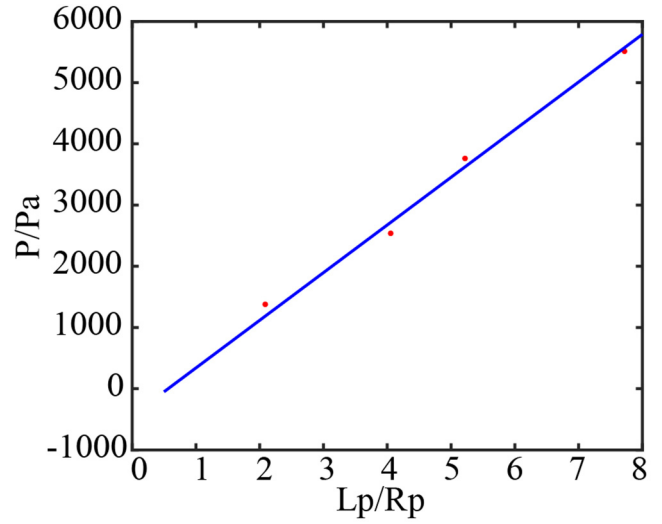


FIG. 14. The relationship between the holding pressure and the elongation of the cytoplasm when its Young's modulus is detected as 762 Pa.

APPENDIX B: OOCYTE RADIUS AND ZP THICKNESS MEASUREMENT

The radius of oocytes and the thickness of ZP were obtained by microscopic image processing. We got the radius of oocytes and cytoplasm by fitting the oocyte and cytoplasm with circles. Then, the thickness of ZP was got by subtracting the values of two radius. Figure 15 shows a figure when the oocyte radius was $75\ \mu\text{m}$ and the thickness of ZP was $17.5\ \mu\text{m}$.

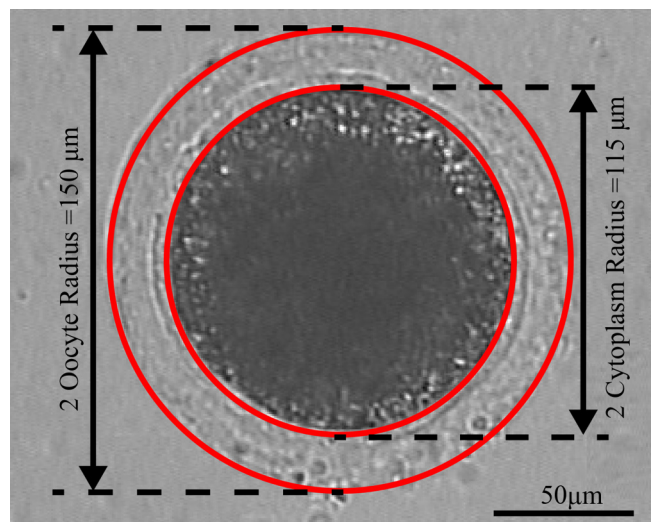


FIG. 15. The oocyte radius was $75\ \mu\text{m}$ and the thickness of ZP was $17.5\ \mu\text{m}$.

APPENDIX C: POINT-LOAD MODEL

The penetration force was estimated according to the point-load model (Fig. 16).²³

According to this model, the penetration force F was estimated by

$$F = \frac{2\pi E h \omega_d^3}{a^2(1-\nu)} \left[\frac{3 - 4\zeta^2 + \zeta^4 + 2\ln\zeta^2}{(1-\zeta^2)(1-\zeta^2 + \ln\zeta^2)^3} \right], \tag{C1}$$

where E is Young’s modulus of ZP, ω_d is the depth created by the penetration force, h is the membrane thickness, a is the radius of dimple, c is the radius of IM, and $\zeta = c/a$. ν is the Poisson ratio which is traditionally set as 0.5.

We calculated the penetration using the point-load model. The calculated magnitude of the penetration force was 10^{-5} N. In the point-load model, the tip of the injection micropipette was flat. The width of the injection micropipette had been taken into consideration to calculate the penetration force. In our experiments, the tip of the injection micropipette was sloped. It is believed that the injection micropipette and the oocyte are contacted by point. Because it takes less force to penetrate a cell with a sloped tip micropipette than it does with a flat tip micropipette, the calculated penetration force was big enough for simulation. The penetration force was a point force in the simulation process.

In our experiments, the tip of the injection micropipette was sloped and sharpened. Thus, the contact between the injection micropipette and the oocyte can be considered as the point of contact. The tip of injection micropipette is flat in the

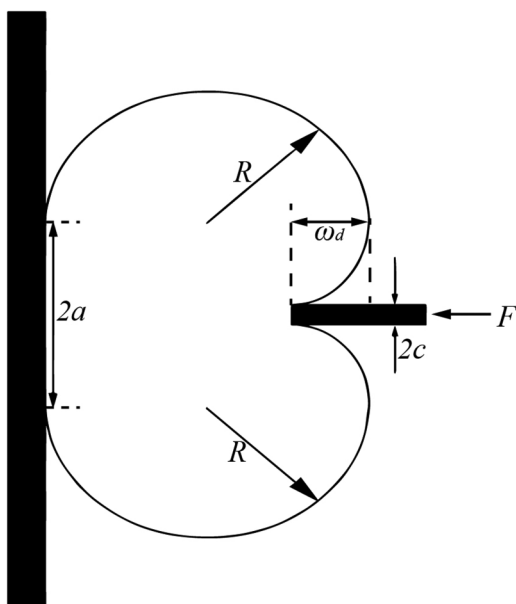


FIG. 16. Schematic of the point-load model.

point-load model and is different with our micropipette. The required penetration force calculated using a flattened micropipette tip in the point-load model is larger than the required penetration force using our micropipette with a sharpened tip. Thus, the calculated force using the point-load model is large enough for simulation. The calculated penetration force was exerted on the central point on the cell surface as shown in Fig. 2.

APPENDIX D: CLEAVAGE RATE DATA

Tables I–III show the detailed cleavage rates at the penetration speed of $10\mu\text{m/s}$, $20\mu\text{m/s}$, and $50\mu\text{m/s}$. The data of the “Experiment 1” in Table III are not available as the oocytes were polluted in that experiment.

TABLE I. Cleavage rate at the penetration speed of $10\mu\text{m/s}$ with different oocyte orientations.

Experiment	Cleavage rates (%)					
	4 o'clock	5 o'clock	6 o'clock	7 o'clock	8 o'clock	9 o'clock
Experiment 1	55.56	46.67	20.69	53.85	65.52	62.96
Experiment 2	60.00	50.00	53.33	3.33	40.00	46.67
Experiment 3	63.33	68.00	80.00	53.57	72.41	63.33
Average	59.63	54.89	51.34	36.92	59.31	57.65

TABLE II. Cleavage rate at the penetration speed of $20\mu\text{m/s}$ with different oocyte orientations.

Experiment	Cleavage rates (%)					
	4 o'clock	5 o'clock	6 o'clock	7 o'clock	8 o'clock	9 o'clock
Experiment 1	84.14	76.67	79.31	80.00	86.67	83.33
Experiment 2	83.33	79.31	54.84	44.83	65.51	83.33
Experiment 3	80.00	70.97	60.00	34.48	70.97	73.33
Average	81.82	75.65	64.72	53.10	74.38	79.99

TABLE III. Cleavage rate at the penetration speed of $50\mu\text{m/s}$ with different oocyte orientations.

Experiment	Cleavage rates (%)					
	4 o'clock	5 o'clock	6 o'clock	7 o'clock	8 o'clock	9 o'clock
Experiment 1
Experiment 2	92.85	86.51	61.53	60.00	80.00	86.67
Experiment 3	80.00	76.67	73.33	63.33	80.00	90.00
Average	86.42	81.59	67.43	61.67	80.00	88.34

REFERENCES

- ¹Z. Liu, Y. J. Cai, Y. Wang, Y. H. Nie, C. C. Zhang, Y. T. Xu, X. T. Zhang, Y. Lu, Z. Y. Wang, M. M. Poo, and Q. Sun, "Cloning of macaque monkeys by somatic cell nuclear transfer," *Cell* **172**, 881 (2018).
- ²A. G. Curcio, F. F. Bressan, F. V. Meirelles, and A. J. B. Dias, "Achievements and perspectives in cloned and transgenic cattle production by nuclear transfer: Influence of cell type, epigenetic status and new technology," *Anim. Reprod.* **14**, 1003 (2017).
- ³Q. L. Zhao, X. Zhao, Y. L. Wang, M. Z. Sun, M. S. Cui, J. Z. Feng, and G. Z. Lu, "Research on autonomous movement of oocyte in nuclei transplantation," *Control Eng. China* **19**, 389 (2012).
- ⁴A. Dinnyes, P. De Sousa, T. King, and I. Wilmut, "Somatic cell nuclear transfer: Recent progress and challenges," *Cloning Stem Cells* **4**, 81 (2002).
- ⁵W. Wang, X. Liu, D. Gelinis, B. Ciruna, and Y. Sun, "A fully automated robotic system for microinjection of zebrafish embryos," *PLoS One* **2**, e862 (2007).
- ⁶J. Park, S. H. Jung, Y. H. Kim, B. Kim, S. K. Lee, and J. O. Park, "Design and fabrication of an integrated cell processor for single embryo cell manipulation," *Lab Chip* **5**, 91 (2005).
- ⁷M. Ammi and A. Ferreira, "Realistic visual and haptic rendering for biological-cell injection," in *Proceedings of the 2005 IEEE International Conference on Robotics and Automation* (IEEE, Barcelona, Spain, 2005), p. 918.
- ⁸A. M. Tabbalat, N. Pereira, D. Klauk, C. Melhem, R. T. Elias, and Z. Rosenwaks, "Arabian peninsula ethnicity is associated with lower ovarian reserve and ovarian response in women undergoing fresh ICSI cycles," *J. Assist. Reprod. Genet.* **35**, 331 (2018).
- ⁹S. Perez-Cerezales, R. Laguna-Barraza, A. C. de Castro, M. J. Sanchez-Calabuig, E. Cano-Oliva, F. J. de Castro-Pita, L. Montoro-Buils, E. Pericuesta, R. Fernandez-Gonzalez, and A. Gutierrez-Adan, "Sperm selection by thermotaxis improves ICSI outcome in mice," *Sci. Rep.* **8**, 2902 (2018).
- ¹⁰P. Stein, and R. M. Schultz, "ICSI in the mouse," *Method Enzymol.* **476**, 251 (2010).
- ¹¹Z. Lu, X. P. Zhang, C. Leung, N. Esfandiari, R. F. Casper, and Y. Sun, "Robotic ICSI (intracytoplasmic sperm injection)," *IEEE Trans. Biomed. Eng.* **58**, 2102 (2011).
- ¹²L. S. Mattos, E. Grant, R. Thresher, and K. Kluckman, "Blastocyst microinjection automation," *IEEE Trans. Inf. Technol. Biomed.* **13**, 822 (2009).
- ¹³A. Scott, K. M. Khan, J. Heer, J. L. Cook, O. Lian, and V. Duronio, "High strain mechanical loading rapidly induces tendon apoptosis: An ex vivo rat tibialis anterior model," *Br. J. Sports Med.* **39**, e25 (2005).
- ¹⁴S. J. Gladman, R. E. Ward, A. T. Michael-Titus, M. M. Knight, and J. V. Priestley, "The effect of mechanical strain or hypoxia on cell death in subpopulations of rat dorsal root ganglion neurons in vitro," *Neuroscience* **171**, 577 (2010).
- ¹⁵L. A. Van der Westerlaken, F. M. Helmerhorst, J. Hermans, and N. Naaktgeboren, "Intracytoplasmic sperm injection: Position of the polar body affects pregnancy rate," *Hum. Reprod.* **14**, 2565 (1999).
- ¹⁶L. Reinzi, F. Ubaldi, F. Martinez, M. Iacobelli, M. G. Minasi, S. Ferrero, J. Tesarik, and E. Greco, "Relationship between meiotic spindle location with regard to the polar body position and oocyte developmental potential after ICSI," *Hum. Reprod.* **18**, 1289 (2003).
- ¹⁷J. Pathak, S. D. Khariche, and A. Goel, "Effects of different activation protocols on cleavage rate and blastocyst production of caprine oocytes," *Iran. J. Vet. Res.* **18**, 243 (2017).
- ¹⁸V. N. Bolton, S. M. Hawes, C. T. Taylor, and J. H. Parsons, "Development of spare human preimplantation embryos in vitro: An analysis of the correlations among gross morphology, cleavage rates, and development to the blastocyst," *J. In Vitro Fert. Embryo Transf.* **6**, 30 (1989).
- ¹⁹L. G. Alexopoulos, M. A. Haider, T. P. Vail, and F. Guilak, "Alterations in the mechanical properties of the human chondrocyte pericellular matrix with osteoarthritis," *J. Biomech. Eng.* **125**, 323 (2003).
- ²⁰M. Khalilian, M. Navidbakhsh, M. R. Valojerdi, M. Chizari, and P. E. Yazdi, "Estimating young's modulus of zona pellucida by micropipette aspiration in combination with theoretical models of ovum," *J. R. Soc. Interface* **7**, 687 (2010).
- ²¹Q. L. Zhao, M. Wu, M. S. Cui, Y. D. Qin, J. Yu, M. Z. Sun, X. Zhao, and X. Z. Feng, "A novel pneumatic micropipette aspiration method using a balance pressure model," *Rev. Sci. Instrum.* **84**, 123703 (2013).
- ²²D. P. Theret, M. J. Levesque, M. Sato, R. M. Nerem, and L. T. Wheeler, "The application of a homogeneous half-space model in the analysis of endothelial cell micropipette measurements," *Trans. ASME* **110**, 190 (1988).
- ²³Y. Sun, K. T. Wan, K. P. Roberts, J. C. Bischof, and B. J. Nelson, "Mechanical property characterization of mouse zona pellucida," *IEEE Trans. Nanobiosci.* **2**, 279 (2003).
- ²⁴Q. L. Zhao, M. Z. Sun, M. S. Cui, J. Yu, Y. D. Qin, and X. Zhao, "Robotic cell rotation based on the minimum rotation force," *IEEE Trans. Autom. Sci. Eng.* **12**, 1504 (2015).
- ²⁵R. O. Duda, and P. E. Hart, "Use of the hough transformation to detect lines and curves in pictures," *Commun. ACM* **15**, 11 (1972).
- ²⁶J. Yu, Q. Zhao, M. Cui, M. Sun, and X. Zhao, "Robotic donor cell injection in somatic cell nuclear transfer (SCNT)," in *Proceeding of the 11th World Congress on Intelligent Control and Automation* (IEEE, Shenyang, China, 2014), p. 2821.
- ²⁷Y. Wang, X. Zhao, Q. Zhao, M. Sun, and G. Lu, "Automatic somatic cell operating process for nuclear transplantation," in *2012 7th IEEE International Conference on Nano/Micro Engineered and Molecular Systems (NEMS)* (IEEE, Kyoto, Japan, 2012).
- ²⁸J. Canny, "A computational approach to edge detection," *IEEE Trans. Pattern Anal. Mach. Intell.* **8**, 679 (1986).
- ²⁹S. Suzuki and K. Abe, "Topological structural analysis of digitized binary images by border following," *Comput. Vis. Graphics Image Process.* **30**, 32–46 (1985).
- ³⁰G. Farneback, "Very high accuracy velocity estimation using orientation tensors, parametric motion, and simultaneous segmentation of the motion field," in *Proceedings Eighth IEEE International Conference on Computer Vision* (IEEE, Vancouver, BC, 2001), Vol. I.
- ³¹C. Zhao, Y. Liu, M. Sun, and X. Zhao, "Robotic cell rotation based on optimal poking direction," *Micromachines* **9**, 141 (2018).
- ³²X. Wang, Y. Liu, S. Li, M. Cui, M. Sun, and X. Zhao, "Automated cell transportation for batch-cell manipulation," in *2017 IEEE/RSJ International Conference on Intelligent Robots and Systems (IROS)* (IEEE, Vancouver, BC, 2017), p. 2974.
- ³³Q. Zhao, B. Shirinzadeh, M. Cui, M. Sun, Y. Liu, and X. Zhao, "A novel cell weighing method based on the minimum immobilization pressure for biological applications," *J. Appl. Phys.* **118**, 044301 (2015).
- ³⁴N. Li, Y. W. Liu, S. B. Li, X. F. Wang, Y. D. Qin, M. Z. Sun, and X. Zhao, "High-precision, pressure-driven pump for sub-picoliter scale quantitative injection," *Mod. Phys. Lett. B* **31**, 1750148 (2017).
- ³⁵Y. Liu, D. Chen, M. Cui, M. Sun, J. Huang, and X. Zhao, "Evaluation of the deformability of the cell's zona pellucida based on the subpixel cell contour detection algorithm," in *2016 35th Chinese Control Conference (CCC)* (IEEE, Chengdu, China, 2016), p. 9109.
- ³⁶A. A. Boulbitch, "Deflection of a cell membrane under application of a local force," *Phys. Rev. E* **57**, 2123 (1998).
- ³⁷E. A. Evans, and R. Skalak, *Mechanics and Thermodynamics of Biomembranes* (CRC Press, 1980).
- ³⁸Y. Tan, D. Sun, W. Huang, and S. H. Cheng, "Mechanical modeling of biological cells in microinjection," *IEEE Trans. Nanobiosci.* **7**, 257 (2008).
- ³⁹H. Ladjal, J.-L. Hanus, and A. Ferreira, "Micro-to-nano biomechanical modeling for assisted biological cell injection," *IEEE Trans. Biomed. Eng.* **60**, 2461 (2013).
- ⁴⁰A. Gabrielsen, S. Lindenberg, and K. Petersen, "The impact of the zona pellucida thickness variation of human embryos on pregnancy outcome in relation to suboptimal embryo development. A prospective randomized controlled study," *Hum. Reprod.* **16**, 2166 (2001).
- ⁴¹K. T. Shiverick, and C. Salafia, "Cigarette smoking and pregnancy I: Ovarian, uterine and placental effects," *Placenta* **20**, 265 (1999).
- ⁴²F. Liu, D. Wu, X. Wu, and K. Chen, "Analyses of the cell mechanical damage during microinjection," *Soft Matter* **11**, 1434 (2015).
- ⁴³H. B. Huang, D. Sun, J. K. Mills, and S. H. Cheng, "Robotic cell injection system with position and force control: Toward automatic batch biomanipulation," *IEEE Trans. Robot.* **25**, 727 (2009).
- ⁴⁴Y. Xie, D. Sun, C. Liu, H. Y. Tse, and S. H. Cheng, "A force control approach to a robot-assisted cell microinjection system," *Int. J. Robot. Res.* **29**, 1222 (2010).